An Efficient Method to Form Heterojunction CdS/TiO2 Photoelectrodes Using Highly Ordered TiO2 Nanotube Array Films

ARTICLE *in* THE JOURNAL OF PHYSICAL CHEMISTRY C · NOVEMBER 2009

Impact Factor: 4.77 · DOI: 10.1021/jp904320d

8 AUTHORS, INCLUDING:

Xianfeng Gao
University of Wisconsin - Milwaukee
24 PUBLICATIONS **1,088** CITATIONS
SEE PROFILE

Lian-Mao Peng
Peking University
394 PUBLICATIONS **9,453** CITATIONS
SEE PROFILE

An Efficient Method To Form Heterojunction CdS/TiO_2 Photoelectrodes Using Highly Ordered TiO_2 Nanotube Array Films

Xian-Feng Gao, Wen-Tao Sun,* Zhu-Dong Hu, Guo Ai, Yi-Ling Zhang, Shi Feng, Fei Li, and Lian-Mao Peng*

Key Laboratory for the Physics and Chemistry of Nanodevices and Department of Electronics, Peking University, Beijing 100871, China

Received: May 8, 2009; Revised Manuscript Received: October 16, 2009

A heterojunction CdS/TiO_2 photoelectrode is prepared by filling CdS nanoparticles into one-dimensional TiO_2 nanotube (NT) array films. The self-assembled TiO_2 NTs are fabricated by an anodization method and sensitized with CdS nanoparticles by the close space sublimation technique. The photoactivity of the as-prepared photoelectrodes was measured in a photoelectrochemical solar cell. Under AM 1.5G illumination, a 5.6 mA/cm^2 short-circuit current density is achieved using the CdS modified photoelectrode, which represents an enhancement by a factor of 36 in photoactivity compared with that of the plain TiO_2 NT array film.

Introduction

Highly ordered, vertically oriented TiO_2 nanotube arrays obtained by Ti anodization have attracted significant interest due to their impressive properties and been explored for applications in such fields as water photoelectrolysis,[1,2] dye-sensitized solar cells,[3−5] gas sensors,[6] and solid-state heterojunction solar cells.[7,8] Compared with the traditional TiO_2 nanocrystals based photoelectrodes, the nanotube array structure based photoelectrode facilitates separation of the photoexcited charges and has higher charge collection efficiency.[9] However, the practical application of TiO_2 NTs is significantly hindered by its wide band gap of 3.2 eV, which limits the photoresponse of TiO_2 to the UV region (which only comprises less than 5% of the solar spectrum). Fortunately, it should be possible to assemble a three-dimensional solar cell based on the TiO_2 NT arrays structure if effective sensitizers or proper electrode materials may be deposited into the TiO_2 NTs. Recently, semiconductors with narrower band gaps, such as CdS,[10−13] PbS,[10,14] Bi_2S_3,[10,15] CdSe,[16,17] CdTe,[18,19] and InP,[20] have been utilized to improve the photoresponse of TiO_2 NTs in the visible region. To fully utilize the internal surfaces of TiO_2 tubes, several methods have been investigated to deposit semiconductor sensitizers into TiO_2 NT electrodes; such methods include electrochemical deposition,[13,18] the sequential chemical bath deposition (S-CBD) method,[12] and a chemical bath method with a bifunctional linker molecule.[17,19,21] These studies indicate that depositing sensitizers into TiO_2 NTs can effectively improve the photoactivity of the electrode in the visible region.

In our earlier papers, we reported that CdS and CdTe quantum dots (QDs) by the chemical bath deposition (CBD) method can be introduced into TiO_2 NTs and be utilized to sensitize and improve significantly the performance of the TiO_2 NT array based photoelectrochemical (PEC) solar systems.[12,19] However, the CBD method is time-consuming and not easy to control. In this paper, we report a facile method to introduce CdS nanoparticles into TiO_2 NTs by the close space sublimation (CSS) technique. The CSS technique offers an easy control over all experimental parameters, and the as-prepared photoelectrode shows a 5.6 mA/cm^2 short-circuit current density, which represents a 36 times enhancement in photoactivity compared with that based on plain TiO_2 NTs. It is expected that this methodology will find applications in designing TiO_2 NT arrays based multijunction solar cells.

SCHEME 1: Schematic Diagram Showing the Synthesis Process of Synthesizing CdS/TiO_2 Heterojunction Photoelectrodes

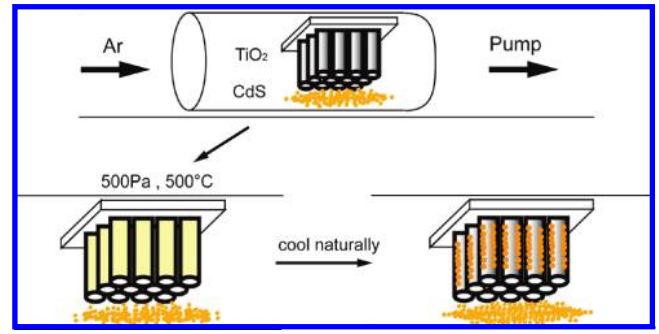

Experimental Section

Fabrication of TiO_2 Nanotube Arrays. The highly ordered TiO_2 NT array films were fabricated by anodic oxidation in NH_4F organic electrolyte, which is similar to that described by Macak et al.[22,23] After oxidation, the samples were ultrasonicated in ethanol to remove the precipitation atop the nanotube films. The so-obtained highly ordered TiO_2 nanotube films were converted into anatase phase by annealing in air for 2 h at 450 °C with heating rates of 3 °C/min.

Deposition of CdS Nanoparticles. High-purity CdS powder (99.99%) with an average size of less than 1 μm was used in this paper and was bought from Chongqing Instrument Material Research Institute (China). In a typical experiment, a TiO_2 nanotube film was placed in a semi-enclosed quartz tube, with an opening end facing down toward the CdS powder, as shown in Scheme 1. The semi-enclosed quartz tube was then transferred into the center of a bigger quartz tube inserted in a horizontal tube furnace. The furnace was pumped by an oil rotary vane

* To whom correspondence should be addressed. E-mail: wtaosun@pku.edu.cn (W.-T.S.), lmpeng@pku.edu.cn (L.-M.P.).

10.1021/jp904320d CCC: $40.75
Published on Web 11/02/2009

vacuum pump (ULVAC GLD-N201) and refilled with high-purity argon (99.999%) for several cycles to eliminate residue oxygen.

Subsequently, a constant flow of high-purity argon (99.999%) was passed through the quartz tube and the system was pumped to a pressure of 500 Pa. The quartz tube was ensured to work at 500 Pa by controlling the pumping rate during the whole process. The temperature of the furnace was rapidly increased to 500 °C and held at that temperature for 30 min. After this process, the furnace was cooled naturally to room temperature.

Characterization of CdS/TiO_2 Heterojunction Photoelectrodes. The structural characterizations of the samples were carried out using a field emission gun FEI XL30 scanning electron microscope (SEM) and a Tecnai G20 transmission electron microscope (TEM). Energy-dispersive X-ray spectroscopy (EDS) was carried out in the TEM. X-ray diffraction (XRD) experiments were carried out by a Philips X'Pert MRD diffractometer to determine the structure of the samples. Reflectance spectra were obtained by using a Shimadzu UV-3100 spectrophotometer over a range of 240−800 nm at a scan speed of 200 nm/min. The photovoltaic performance of the CdS QD-sensitized TiO_2 nanotube film was measured in a PEC cell with a Pt thread counter electrode and Ag/AgCl reference electrode. A 0.1 M Na_2S aqueous solution was used as the electrolyte to maintain the stability of the CdS nanoparticles. The samples were pressed against an O-ring in the photoelectrochemical cell, leaving an area of 0.515 cm^2 exposed to the light source. The photocurrent density−voltage (J−V) characteristics measurements were performed under AM 1.5 simulated sunlight which was produced by a 300 W Oriel solar simulator (model 91160) with an illumination intensity of 138.4 mW/cm^2. An electrochemical analyzer (CHI660C Instruments) was used to record the photocurrent and photovoltage. The J−V scan was performed from −1.3 to 0 V with a scanning rate of 5 mV/s. All optical and electrochemical tests were carried out under ambient conditions.

Result and Discussion

Morphologies of TiO_2 Nanotube Arrays. Self-organized and vertically oriented TiO_2 NT arrays were obtained by anodization of Ti film. Low- and a high-magnification SEM images showing the morphologies of the TiO_2 NT array film are shown, respectively, in Figure 1a,b. The images show that TiO_2 NT arrays have a close-packed structure and the average nanotube diameter is about 140 nm. The tube structure is uniform over a wide area (Figure 1a). The inset of Figure 1a is a cross-sectional image showing that the NTs are well aligned with an average length of about 27.5 μm.

Structure of CdS-Modified TiO_2 Nanotube Arrays. The surface morphology of modified TiO_2 NT arrays was examined by SEM. Figure 2a shows that the surface of the modified TiO_2 NT arrays is not destroyed by the deposition process and the pores of the TiO_2 NTs are not blocked by CdS particles. Figure 2b is a higher-magnification SEM image, showing that many CdS nanoparticles are introduced onto the side wall of TiO_2 NTs. The inset of Figure 2a is a cross-sectional view of the CdS-deposited TiO_2 nanotube arrays, revealing that there also exist some CdS particles on the outer walls of TiO_2 NTs.

To clarify whether or not the CdS particles were introduced deep into the TiO_2 nanotubes, the CdS/TiO_2 hybrid structure was further investigated by TEM. TEM images of TiO_2 NTs (Figure 3) give a clear comparison of the TiO_2 NTs before and after CdS deposition. Figure 3a illustrates a single TiO_2 NT, and the right inset of Figure 3a shows a high-magnification

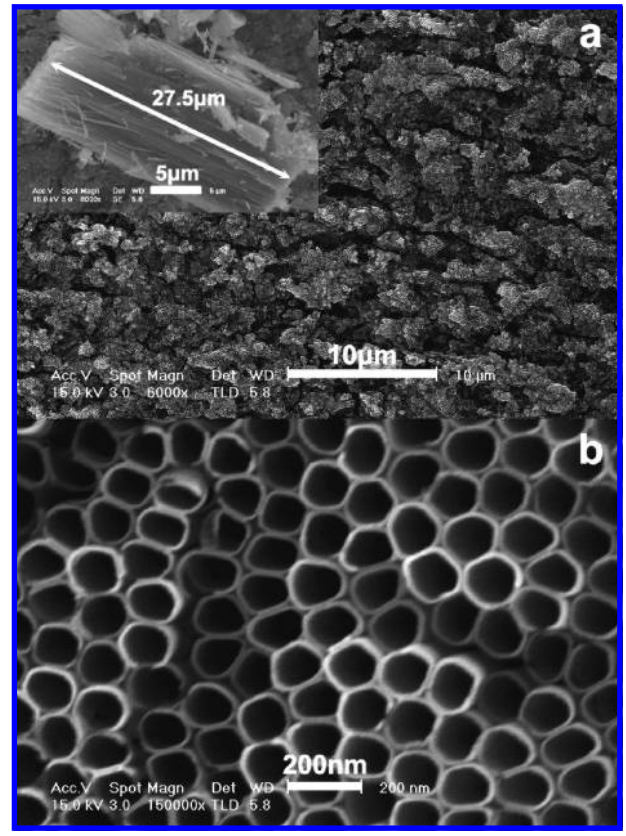

Figure 1. SEM images of TiO_2 nanotube arrays with low (a) and high (b) magnifications. The inset is a cross-sectional SEM image of the film.

image of the TiO_2 NT before CdS deposition. The tube wall is very smooth, and no nanoparticles are seen inside the tube. Lattice fringes of 0.352 nm are observed in the HR-TEM image of the TiO_2 NT (left inset of Figure 3a), which corresponds to the (101) plane of anatase (JCPDS file no. 71-1167), suggesting that the TiO_2 nanotube is well-crystallized. Figure 3b is a TEM image of the TiO_2 NTs after the deposition of CdS particles, showing that the CdS particles have been deposited along the tube wall, and the particle size is around 20 nm. The high-resolution TEM image (left inset of Figure 3b) of the deposited CdS nanoparticles indicates that the CdS nanoparticles are well-crystallized, and the marked 0.358 nm spacing corresponds to the (100) lattice plane of CdS (JCPDS file no.77-2306). The sample composition was identified by EDS analysis (Figure 3c) performed inside the TEM. The Cu and C peaks are derived from the supporting amorphous carbon film on a Cu grid. Besides Ti and O peaks from TiO_2 NTs, Cd and S peaks in the EDS spectrum reveal that the particles deposited inside TiO_2 NTs are mainly composed of cadmium and sulfur. Quantitative analysis of the EDS spectrum gives a Cd/S atomic ratio of about 1, indicating that high-grade CdS particles were formed inside the TiO_2 NTs.

The crystal structure of the deposited CdS was examined by X-ray diffraction experiments. For comparison, an X-ray diffraction pattern from the plain TiO_2 NT sample is also given. As shown in Figure 4, pattern a, all diffraction peaks can be well-indexed by the anatase phase of TiO_2 (JCPDS file no. 71-1167, marked by A) and Ti metal phase (JCPDS file no. 05-0682, marked by T). These peaks are originated from the TiO_2 nanotube film and Ti substrate, respectively. The crystallization of the TiO_2 NT is in agreement with that shown in the TEM images of Figure 3. Besides TiO_2 and Ti diffraction peaks, also

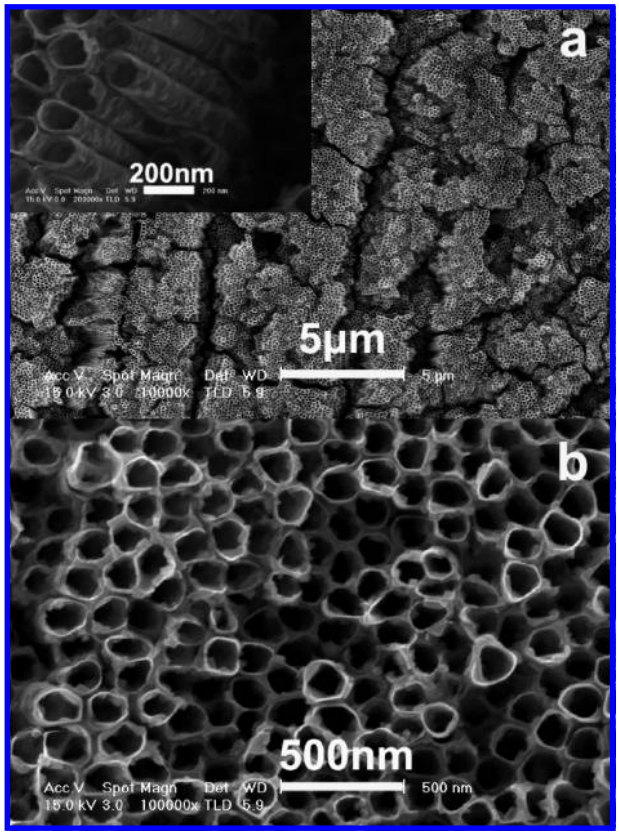

Figure 2. SEM images of TiO_2 nanotube arrays after CdS deposition with low (a) and high (b) magnification. The inset is a cross-sectional SEM image of the modified film.

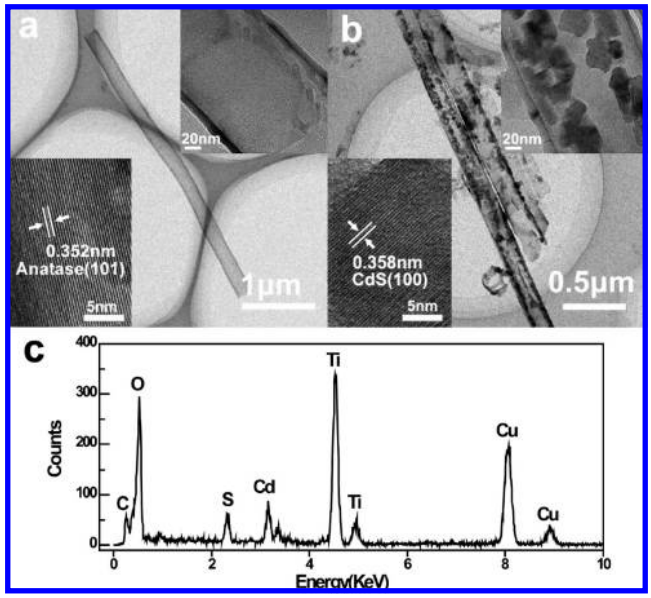

Figure 3. TEM images of individual TiO_2 nanotubes before (a) and after (b) CdS deposition. The right insets are high-magnification images. The left inset of (a) is a HR-TEM image of TiO_2. The left inset of (b) is a HR-TEM image of the deposited CdS nanoparticle. (c) EDS spectrum of the CdS/TiO_2 NT.

presented in Figure 4, pattern b, are CdS peaks (JCPDS file no.77-2306, marked by C), and these peaks reveal that the CdS particles actually have the hexagonal structure that is in agreement with that revealed by the high-resolution TEM image (left inset of Figure 3). The X-ray diffraction pattern also confirms that no significant Cd- or S-related impurities are present in the deposited particles.

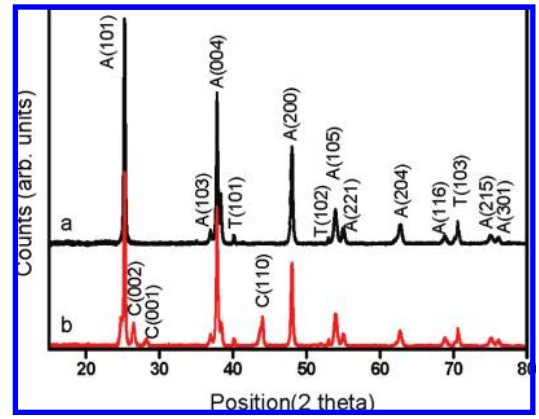

Figure 4. Experimental XRD profiles obtained from plain TiO_2 (a) and CdS/TiO_2 NT film (b). The peaks are denoted by A = TiO_2 anatase (JCPDS file no. 71-1167), T = metal titanium substrate (JCPDS file no. 05-0682), and C = CdS hexagonal phase (JCPDS file no. 77-2306).

Growth Mechanism. The CSS technique has been used to deposit CdS films.[24,25] The growth mechanism of CdS nanoparticle deposition is quite similar to that of CdS film deposition. The typical sublimated temperature of CdS in the CSS technique is above 650 °C. However, in our work, the low gas pressure ensures that CdS powder can sublimate at a relative lower reaction temperature (500 °C), which protects the TiO_2 NT substrate from disruption. The formation process of the CdS/TiO_2 NT photoelectrode is depicted in Scheme 1. The formation of CdS nanoparticles may be attributed to the vapor−solid growth mechanism. According to an earlier study, CdS gas will decompose to Cd gas and S_2 gas at high temperature.[24] When the reaction chamber was heated to 500 °C quickly at a pressure of 500 Pa, the chemical reaction may be described by the following equations

$$CdS(s) \rightarrow CdS(g) \quad (1)$$

$$2CdS(g) \rightarrow 2Cd(g) + S_2(g) \quad (2)$$

The unceasing evaporation leads to a relative higher pressure near the CdS source than that around the TiO_2 nanotube film. Cd and S vapor infiltrate into TiO_2 NTs because of the gas pressure gradient. The CdS decomposing process is predominant until the sublimation and desublimation process become equilibrium after several minutes. As a result, the TiO_2 NTs are filled with CdS vapor and the supersaturation increases until the nuclei form. As the temperature of the furnace decreases naturally to a suitable temperature region, the vapor mixture undergoes a fast condensation reaction process and recombines to form crystalline CdS nanocrystals inside the TiO_2 NTs.

$$2Cd(g) + S_2(g) \rightarrow 2CdS(s) \quad (3)$$

In fact, a similar vapor−solid growth mechanism also works in the growth of CdS nanowires[26] and ZnSe nanobelts.[27]

Photoresponse of the CdS/TiO_2 Hybrid Structure. Shown in Figure 5 are reflectance spectra recorded from the TiO_2 NT arrays before (a) and after (b) CdS deposition. It can be seen from these spectra that both samples exhibited low reflectance (below 25%) in the whole UV and visible region, which may be attributed to the lower index of refraction and multiple scattering in the one-dimensional nanomaterials.[28−30] For the

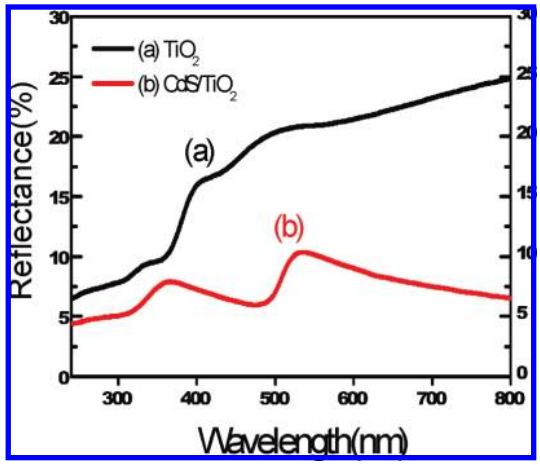

Figure 5. Reflectance spectra of the TiO_2 nanotube arrays before (a) and after (b) CdS deposition.

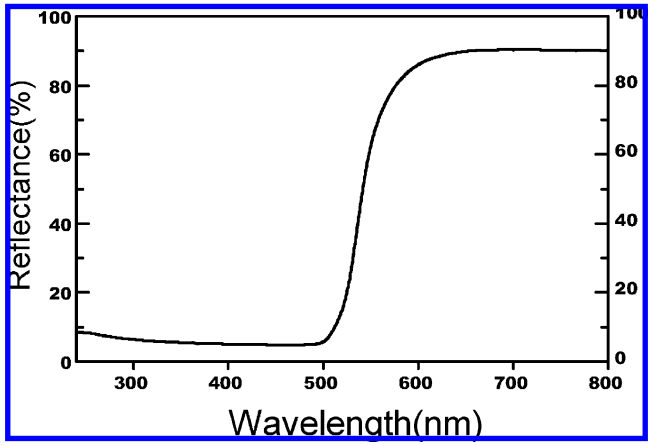

Figure 6. Reflectance spectrum of the TiO_2 nanotube arrays covered with a CdS film.

TiO_2 NT array film, the diffuse reflectance decreases strongly below 400 nm, which is due to the strong intrinsic optical absorption of TiO_2 (curve a in Figure 5). For the hybrid structure of CdS/TiO_2, the reflectance is much lower than that of the plain TiO_2 NT arrays and decreases strongly at 520 nm. This strong decrease in visible reflection is due to the strong absorption of visible light by the deposited CdS particles. It is thus demonstrated that the hybrid structure may effectively improve the photoactivity of the TiO_2 electrode by enhancing visible-light absorption. To confirm the enhanced antireflection behavior of the CdS/TiO_2 heterojunction, a CdS film was produced on the surface of the TiO_2 NT film with the doctor blading method. This as-prepared CdS-TiO_2 film shows a very strong reflectance of about 90% in the long wavelength region (Figure 6). This result demonstrates that, when the TiO_2 NT array is covered with CdS film, light scattering within the NT array becomes negligible. The decrease of reflectance at the short wavelength region (below ~520 nm) may be attributed to the strong intrinsic absorption of CdS. It is thus shown that effective antireflection exists only when CdS nanoparticles were deposited into the TiO_2 NT. The CdS nanoparticles' deposition increased the roughness of the TiO_2 NTs' surface and, therefore, enhanced light scattering, which contributes to the antireflection and light absorption. The effective antireflection of the CdS/TiO_2 heterojunction photoelectrode results from the combination of multiple scattering with strong optical absorption of CdS nanoparticles in the visible region.

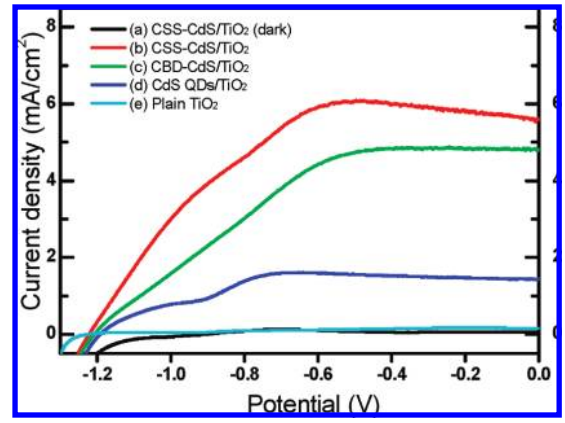

Figure 7. Current density−voltage characteristics measured from the CdS/TiO_2 photoelectrode made by the CSS technique under dark condition (a) and under AM 1.5G illuminations (b). For comparison, photocurrents obtained from a plain TiO_2 nanotube film (e) and a CdS/TiO_2 photoelectrode made by the CBD method (c) and presynthesized QD deposition (d) are also given.

Photoelectrochemical Activity. In addition to enhanced light absorption, the formation of a CdS/TiO_2 heterojunction in the hybrid structure also facilitates separation of the photogenerated electrons and holes.[12,13,31] The experimental J−V characteristics measured from the CdS/TiO_2 photoelectrode are shown in Figure 7. For a comparison, the photoactivity of a plain TiO_2 NT electrode and CdS/TiO_2 hybrid ones fabricated with two other CdS deposition methods are also illustrated in the same figure. Curve c (Figure 7) refers to the case where CdS particles were synthesized and deposited in situ by CBD.[12] Curve d (Figure 7) refers to the case where CdS QDs were presynthesized via a method similar to that described by Yu et al.[32] and deposited by a linker molecule (mercaptopropionic acid (MPA)[17,19]). Detailed information about the other two deposition methods can be found in our earlier paper.[12,19] All relevant parameters, including electrode area, morphology, and crystallization of the TiO_2 substrate, are the same for all the three types of CdS/TiO_2 photoelectrodes.

For all cases, the CdS/TiO_2 NTs did not show any significant activity in the dark, giving a short-circuit current (I_{SC}) of only 0.06 mA/cm^2. On the other hand, under AM 1.5G illumination, an I_{SC} of 5.6 mA/cm^2 was obtained for the CdS-modified TiO_2 NT electrode via the CSS method. Compared with the plain TiO_2 NT electrode, which gives a short-circuit photocurrent of 0.15 mA/cm^2, this presents a significant increase of photoactivity. Among the three deposition methods, the CdS/TiO_2 photoelectrode made by the CSS technique has the highest short-circuit photocurrent. This improvement is caused by the different attachment modes between CdS and TiO_2 NTs. It has been proven that a direct contact or close proximity between the QD sensitizer and TiO_2 is beneficial for the efficiency of the photoanode.[33] CdS/TiO_2 formed with the CBD method also shows good photoactivity and resulted in a photocurrent of 4.8 mA/cm^2. Because CdS particles deposited by both CSS and CBD techniques have a good direct contact with TiO_2 NTs, the resulted photocurrents are of the same order of magnitude (5.6 versus 4.8 mA/cm^2). Figure 7 shows clearly that CdS nanoparticles contribute significantly to the photoresponse improvement of the TiO_2 NTs based electrode, and the CSS technique is an efficient method to introduce semiconducting QD sensitizers into, and form good interface with, the TiO_2 NTs.

Because the conduction band edge of CdS is above that of the TiO_2 nanotube, when CdS is combined with TiO_2, local band

bending occurs at the CdS/TiO_2 interface and a local electric field is established. When illuminated, CdS effectively absorbs visible light and excites electrons and holes pairs. The local electric field at the CdS/TiO_2 interface pushes the photon-generated electrons (holes) toward the conduction (valence) band of TiO_2 (CdS); the photoexcited electrons can be effectively collected by TiO_2 and holes by CdS. Because the TiO_2 NTs are crystalline and well-aligned on the Ti substrate, the injected electrons can be transferred effectively to the collector electrode (the Ti substrate foil). Therefore, besides visible-light absorption, the heterojunction CdS/TiO_2 photoelectrode also facilitates separation of the photogenerated electrons and holes and, subsequently, improves the photoactivity of the TiO_2 NT photoelectrode.

It should be noted that sulfur doping can also improve the photocatalytic activity of TiO_2.[34] Although S or Cd atoms might exist in TiO_2 nanotubes after heat treatment, extensive observations carried out in TEM did not show any S or Cd particles; instead, many CdS particles were observed. Furthermore, no evident peaks were found that correspond to neither Cd nor S in the XRD profiles obtained from the CdS/TiO_2 electrode. We thus conclude that no large amount of Cd or S particles was deposited into the TiO2 film and that the significant improvement of photoactivity is resulted mainly from the CdS nanoparticle deposition and the formation of the CdS/TiO_2 heterojunction.

Conclusion

In summary, the close space sublimation technique has been used to deposit CdS nanocrystals into TiO_2 NT photoelectrodes. The as-prepared CdS/TiO_2 heterojunction electrode leads to better solar light harvesting in the visible-light region. A 5.6 mA/cm^2 photocurrent is obtained in a photoelectrochemical solar cell, which presents an enhancement by a factor of 36 compared with that of the plain TiO_2 NT electrode.

Acknowledgment. This work was supported by the Ministry of Science and Technology (Grant No. 2006CB932401) and the National Science Foundation of China (Grant Nos. 90606026 and 60871002). We thank Prof. Tang Fangqiong and Mr. Li Hongbo for providing CdS QDs.

References and Notes

(1) Mor, G. K.; Shankar, K.; Paulose, M.; Varghese, O. K.; Grimes, C. A. *Nano Lett.* **2005**, *5*, 191.
(2) Park, J. H.; Kim, S.; Bard, A. J. *Nano Lett.* **2006**, *6*, 24.
(3) Mor, G. K.; Shankar, K.; Paulose, M.; Varghese, O. K.; Grimes, C. A. *Nano Lett.* **2006**, *6*, 215.
(4) Paulose, M.; Shankar, K.; Varghese, O. K.; Mor, G. K.; Hardin, B.; Grimes, C. A. *Nanotechnology* **2006**, *17*, 1446.
(5) Zhu, K.; Vinzant, T. B.; Neale, N. R.; Frank, A. J. *Nano Lett.* **2007**, *7*, 3739.
(6) Paulose, M.; Varghese, O. K.; Mor, G. K.; Grimes, C. A.; Ong, K. G. *Nanotechnology* **2006**, *17*, 398.
(7) Shankar, K.; Mor, G. K.; Prakasam, H. E.; Varghese, O. K.; Grimes, C. A. *Langmuir* **2007**, *23*, 12445.
(8) Mor, G. K.; Shankar, K.; Paulose, M.; Varghese, O. K.; Grimes, C. A. *Appl. Phys. Lett.* **2007**, *91*, 152111.
(9) Zhu, K.; Neale, N. R.; Miedaner, A.; Frank, A. J. *Nano Lett.* **2007**, *7*, 69.
(10) Vogel, R.; Hoyer, P.; Weller, H. *J. Phys. Chem.* **1994**, *98*, 3183.
(11) Lin, S. C.; Lee, Y. L.; Chang, C. H.; Shen, Y. J.; Yang, Y. M. *Appl. Phys. Lett.* **2007**, *90*, 143517.
(12) Sun, W. T.; Yu, Y.; Pan, H. Y.; Gao, X. F.; Chen, Q.; Peng, L. M. *J. Am. Chem. Soc.* **2008**, *130*, 1124.
(13) Banerjee, S.; Mohapatra, S. K.; Das, P. P.; Misra, M. *Chem. Mater.* **2008**, *20*, 6784.
(14) Plass, R.; Pelet, S.; Krueger, J.; Gratzel, M. *J. Phys. Chem. B* **2002**, *106*, 7578.
(15) Peter, L. M.; Wijayantha, K. G. U.; Riley, D. J.; Waggett, J. P. *J. Phys. Chem. B* **2003**, *107*, 8378.
(16) Shen, Q.; Sato, T.; Hashimoto, M.; Chen, C.; Toyoda, T. *Thin Solid Films* **2006**, *499*, 299.
(17) Robel, I.; Subramanian, V.; Kuno, M.; Kamat, P. V. *J. Am. Chem. Soc.* **2006**, *128*, 2385.
(18) Seabold, J. A.; Shankar, K.; Wilke, R. H. T.; Paulose, M.; Varghese, O. K.; Grimes, C. A.; Choi, K. S. *Chem. Mater.* **2008**, *20*, 5266.
(19) Gao, X. F.; Li, H. B.; Sun, W. T.; Chen, Q.; Tang, F. Q.; Peng, L. M. *J. Phys. Chem. C* **2009**, *113*, 7531.
(20) Zaban, A.; Micic, O. I.; Gregg, B. A.; Nozik, A. J. *Langmuir* **1998**, *14*, 3153.
(21) Kongkanand, A.; Tvrdy, K.; Takechi, K.; Kuno, M.; Kamat, P. V. *J. Am. Chem. Soc.* **2008**, *130*, 4007.
(22) Macak, J. M.; Tsucak, H.; Schmuki, P. *Angew. Chem., Int. Ed.* **2005**, *44*, 2100.
(23) Macak, J. M.; Tsuchiya, H.; Taveira, L.; Aldabergerova, S.; Schmuki, P. *Angew. Chem., Int. Ed.* **2005**, *44*, 7463.
(24) Mejia-Garcia, C.; Escamilla-Esquivel, A.; Contreras-Puente, G.; Tufino-Velazquez, M.; Albor-Aguilera, M. L.; Vigil, O.; Vaillant, L. *J. Appl. Phys.* **1999**, *86*, 3171.
(25) Moutinho, H. R.; Albin, D.; Yan, Y.; Dhere, R. G.; Li, X.; Perkins, C.; Jiang, C. S.; To, B.; Al-Jassim, M. M. *Thin Solid Films* **2003**, *436*, 175.
(26) Shen, G. Z.; Lee, C. J. *Cryst. Growth Des.* **2005**, *5*, 1085.
(27) Hu, Z. D.; Duan, X. F.; Gao, M.; Chen, Q.; Peng, L. M. *J. Phys. Chem. C* **2007**, *111*, 2987.
(28) Hu, L.; Chen, G. *Nano Lett.* **2007**, *7*, 3249.
(29) Muskens, O. L.; Rivas, J. G.; Algra, R. E.; Bakkers, E. P. A. M.; Lagendijk, A. *Nano Lett.* **2008**, *8*, 2638.
(30) Lee, Y. J.; Ruby, D. S.; Peters, D. W.; McKenzie, B. B.; Hsu, J. W. P. *Nano Lett.* **2008**, *8*, 1501.
(31) Tachibana, Y.; Umekita, K.; Otsuka, Y.; Kuwabata, S. *J. Phys. Chem. C* **2009**, *113*, 6852.
(32) Yu, W. W.; Peng, X. G. *Angew. Chem., Int. Ed.* **2002**, *41*, 2368.
(33) Guijarro, N.; Lana-Villarreal, T.; Mora-Sero, I.; Bisquert, J.; Gomez, R. *J. Phys. Chem. C* **2009**, *113*, 4208.
(34) Tang, X. H.; Li, D. Y. *J. Phys. Chem. C* **2008**, *112*, 5405.

JP904320D